Fig S1. Separation of LotA deubiquitinase activities

A

OTU	$LotA_N$	$LotA_M$	LotB	LotC	LotD
$LotA_N$	100	23	20	22	27
$LotA_M$	23	100	18	28	45
LotB	20	18	100	21	19
LotC	22	28	21	100	28
LotD	27	45	19	28	100

B

Insertion	$LotA_N$	$LotA_M$	LotB	LotC	LotD
$LotA_N$	100	19	13	17	21
$LotA_M$	19	100	17	16	27
LotB	13	17	100	12	20
LotC	17	16	12	100	20
LotD	21	27	20	20	100

C

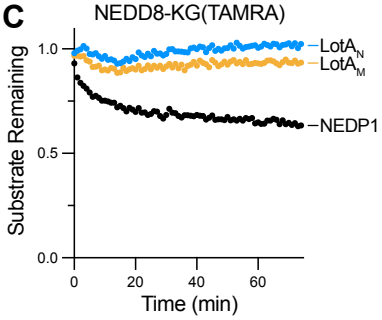

D

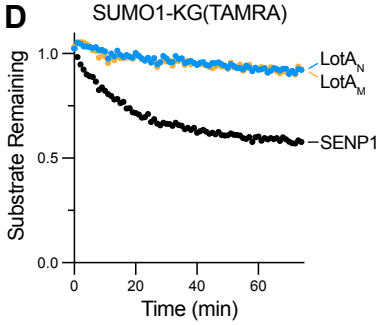

E

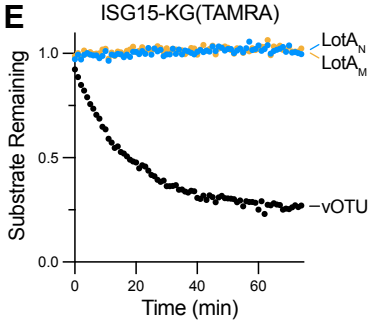

Supplementary Figure 1: Separation of LotA deubiquitinase activities, related to Figure 1

A. Pairwise sequence identity matrix calculated from a T-Coffee multiple sequence alignment[1] performed on the Lot-class core OTU domain sequences following structure-guided removal of the insertion domains.

B. As in (**A**), for the Lot-class insertion domains.

C-E. Ub-like-KG(TAMRA) cleavage assays for NEDD8 (**C**), SUMO1 (**D**), and ISG15 (**E**) monitored by fluorescence polarization. Activity was measured using 1 μM $LotA_N$, 1 μM $LotA_M$. 6 nM NEDP1, 250 pM SENP1, and 400 nM vOTU were used as control enzymes for NEDD8, SUMO1, and ISG15, respectively.

Fig S2. Application of $LotA_N$ K6 specificity for UbiCRest analysis

A

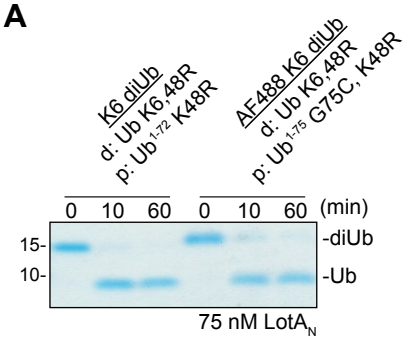

B

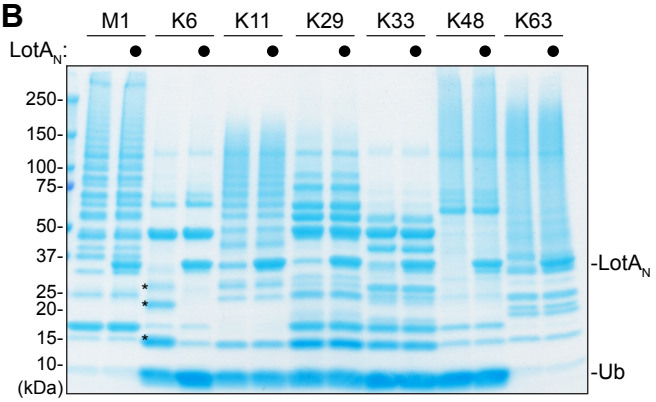

Supplementary Figure 2: Application of LotA$_N$ K6 specificity for UbiCRest analysis, related to Figure 2

A. Gel-based LotA$_N$ cleavage assay comparing the capped and fluorescent capped K6 diUb substrates used in the kinetic analysis. Capped K6 diUb incorporated the annotated mutations into the distal (d) and proximal (p) Ub moieties to streamline production.

B. Homogeneous assemblies for seven polyUb linkage types were generated and treated with a high concentration (5 μM) of LotA$_N$ for 2 h before the reactions were quenched, resolved by SDS PAGE, and visualized for cleavage by Coomassie staining. In the LotA$_N$ treatment of K6 polyUb, all observed polyUb bands are indicated with asterisks. All LotA$_N$-resistant protein bands in the K6 polyUb treatment are enzymes used in the substrate assembly process.

Fig S3. Crystal structure of the $LotA_N$ OTU domain

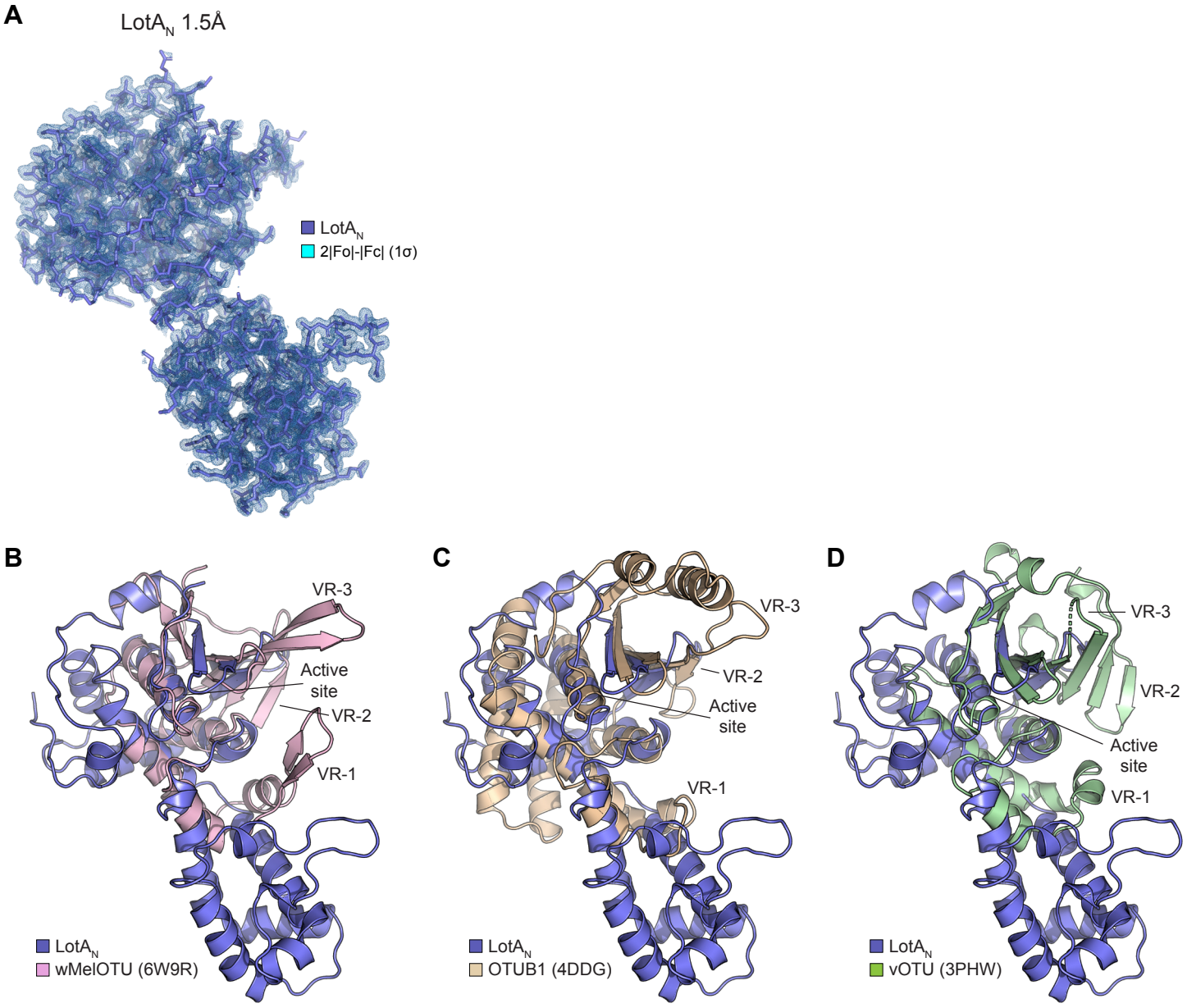

Supplementary Figure 3: Crystal structure of the $LotA_N$ OTU domain, related to Figure 3

A. 1.5Å crystal structure of $LotA_N$ (1-294). The $LotA_N$ model is shown in sticks with 2|Fo|-|Fc| electron density overlaid at 1σ.

B. Structural overlay of $LotA_N$ (blue) with wMelOTU (pink) from *Wolbachia pipientis* wMel (PDB 6W9R). The aligned active sites are annotated and the unique variable regions of wMelOTU are indicated.

C. Structural overlay of $LotA_N$ (blue) with human OTUB1 (PDB 4DDG, tan). The aligned active sites are annotated and the unique variable regions of OTUB1 are indicated.

D. Structural overlay of $LotA_N$ (blue) with vOTU (green) from CrimeanCongo hemorrhagic fever virus (PDB 3PHW). The aligned active sites are annotated and the unique variable regions of vOTU are indicated.

Fig S4. Crystal structure of the LotA$_N$ OTU domain bound to K6 diUb

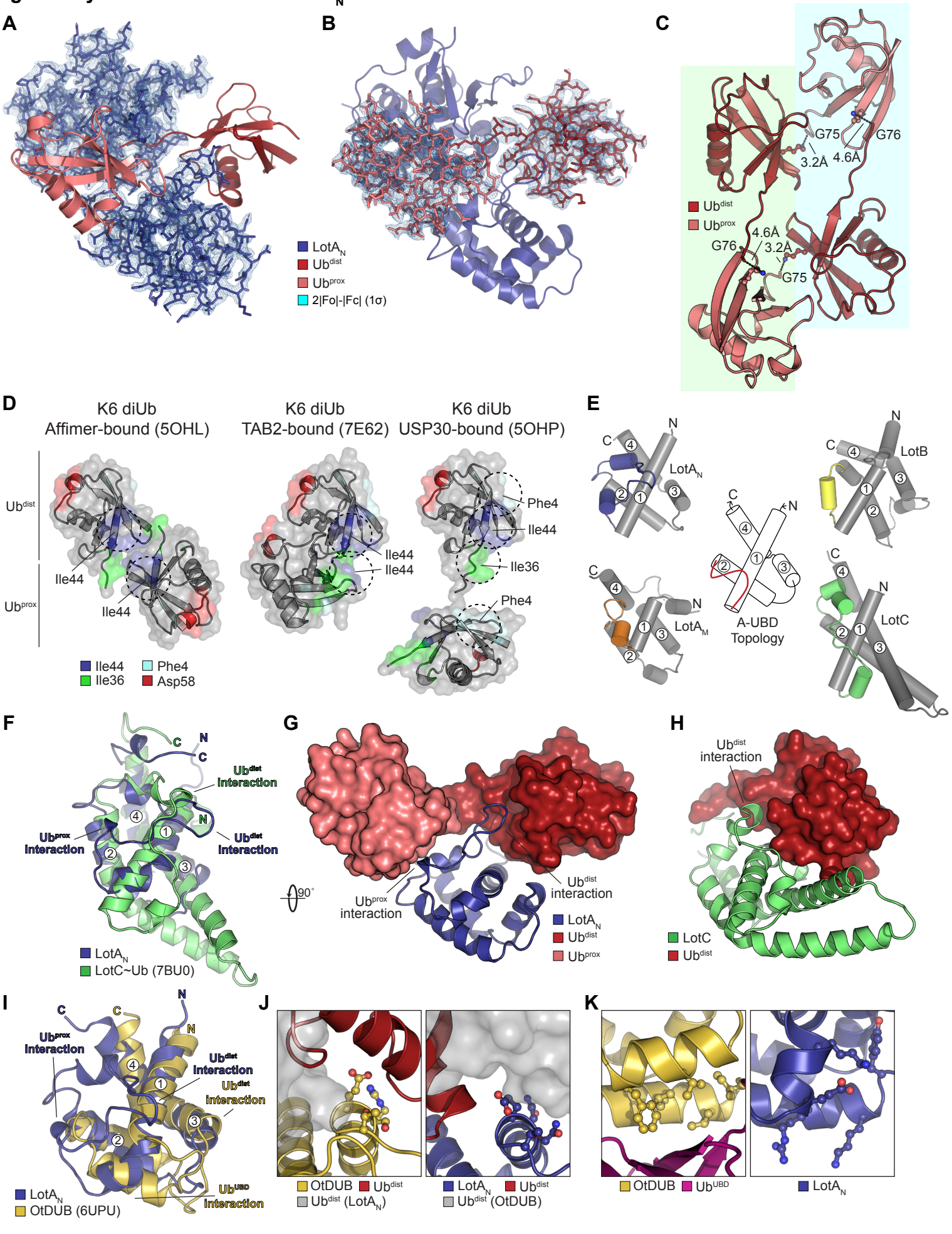

Supplementary Figure 4: Crystal structure of the $LotA_N$ OTU domain bound to K6 diUb, related to Figure 4

A. 2.8Å crystal structure of $LotA_N$ (1-276) bound to K6 diUb. The $LotA_N$ model (blue) is shown in sticks with 2|Fo|-|Fc| electron density overlaid at 1σ, while the K6 diUb model (shades of red) is shown in cartoon.

B. 2.8Å crystal structure of $LotA_N$ (1-276) bound to K6 diUb. The K6 diUb model (shades of red) is shown in sticks with 2|Fo|-|Fc| electron density overlaid at 1σ, while the $LotA_N$ model (blue) is shown in cartoon.

C. Cartoon representation of symmetry-related K6 diUb molecules. Distances between the Ub^{dist} C-terminus and Ub^{prox} K6 are shown within (blue or green) or across asymmetric units (blue to green).

D. Crystal structures of K6 diUb bound to a K6-specific affimer (PDB 5OHL), TAB2 (PDB 7E62), or USP30 (PDB 5OHP), aligned by their distal Ub moieties (top) and shown side-by-side. Availability and orientation of common interaction surfaces are shown, with dashed circles indicating the surfaces utilized by protein interfaces.

E. Underlying helical domain architecture of the Lot-class A-UBDs, with helices labeled and the Ub-binding α1-2 regions shown in color.

F. Structural overlay of A-UBDs from $LotA_N$ (blue) and LotC (green), with helices and Ub interaction surfaces labeled.

G. Rotated view of the interaction between the $LotA_N$ A-UBD (blue, cartoon) and K6 diUb (surface, shades of red), with Ub interaction surfaces labeled.

H. Rotated view of the interaction between the LotC A-UBD (green, cartoon) and a Ub bound in the S1 site (surface, red), with Ub interaction surfaces labeled.

I. Structural overlay of the A-UBDs from $LotA_N$ (blue) and *Orientia tsutsugamushi* OtDUB (PDB 6UPU, gold), with helices and Ub interaction surfaces labeled.

J. Side-by-side view of the OtDUB Ub^{dist} interaction surface on Helix 3 (gold) alongside the analogous, conserved region of $LotA_N$ (blue). The bound Ub^{dist} molecules (red) would clash with additional Ub molecules (gray surface) overlaid from the opposite protein structure.

K. Side-by-side view of the OtDUB Ub^{UBD} high affinity interaction site in the α1-2 region (gold) bound to Ub (maroon), alongside the distinct α1-2 region of $LotA_N$ (blue).

Fig S5. Conformational changes of $LotA_N$ during catalysis

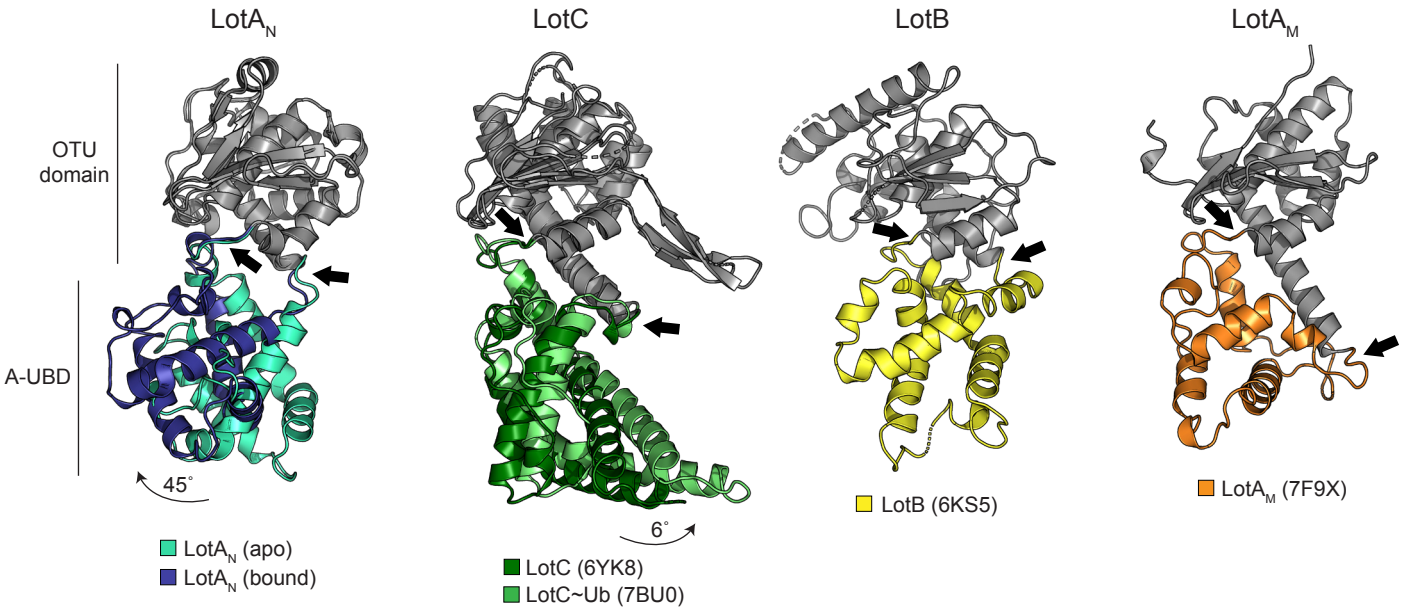

Supplementary Figure 5: Conformational changes of $LotA_N$ during catalysis, related to Figure 5

Side view of all structurally-characterized Lot-class DUBs highlighting hinge movement upon Ub binding for $LotA_N$ (blue) and LotC (green), and putative hinge regions in the $LotA_M$ (orange) and LotB (yellow) structures. Hinge regions between the OTU domain and A-UBD are indicated with black arrows.

Fig S6. LotA$_N$ restriction of K6 polyUb during *L. pneumophila* infection

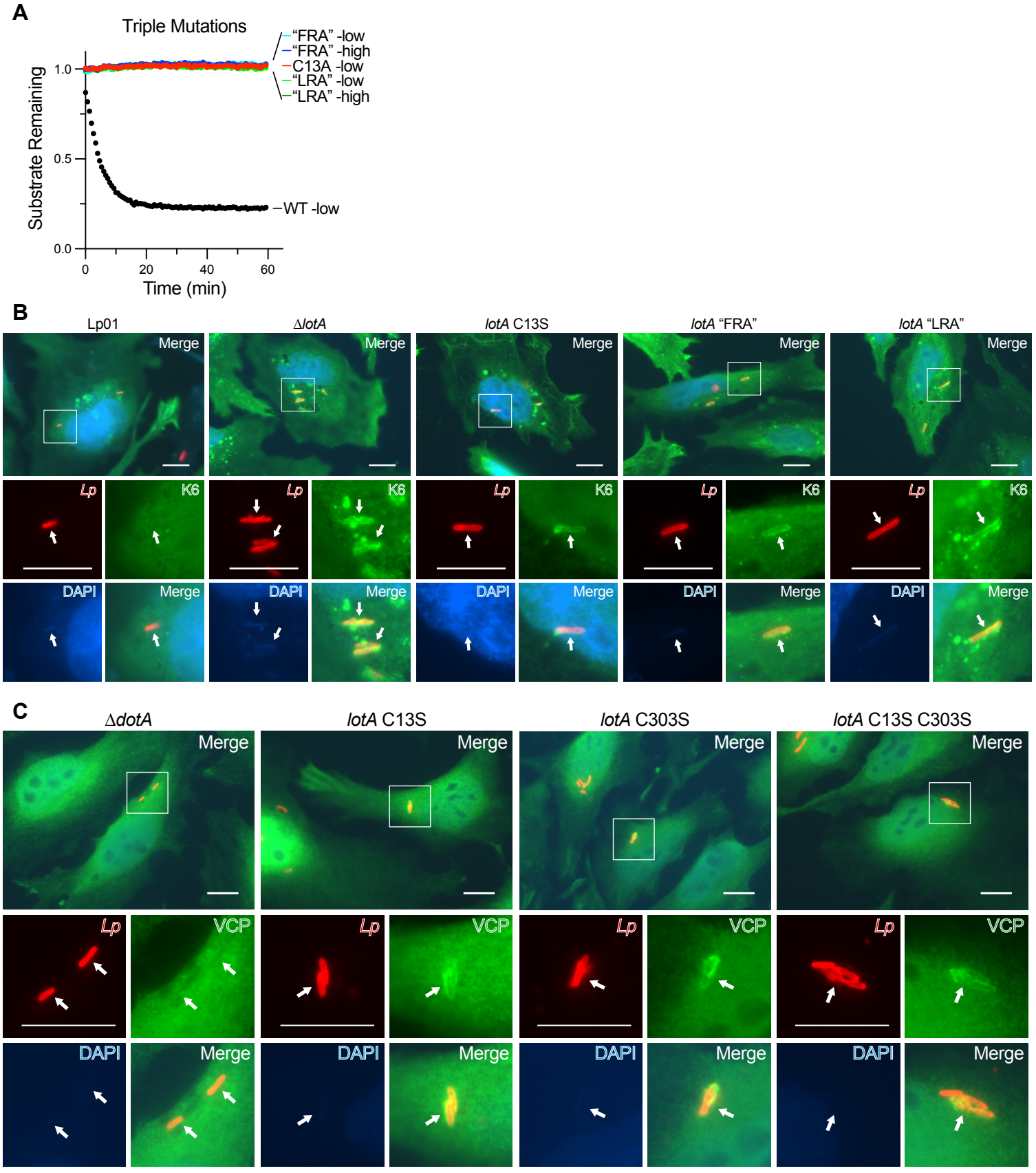

Supplementary Figure 6: LotA$_N$ restriction of K6 polyUb during *L. pneumophila* infection, related to Figure 6

A. Cleavage of K6 diUb by the indicated LotA$_N$ variants at 10 nM (low) or 1 μM (high) concentration monitored by fluorescence polarization. The "FRA" triple mutant combines the LotA$_N$ S1'-site F120A, S1'-site R145L, and hinge A193P mutations. The "LRA" triple mutant combines the LotA$_N$ S1-site L128R, S1'-site R145L, and hinge A193P mutations. These data were collected in parallel with those presented in Fig. 3C, and the WT dataset is shown again for reference.

B. Representative images of HeLa FcγRII cells infected with the indicated *L. pneumophila* strains at an MOI of 2 for 4 h. Fixed cells were stained for *L. pneumophila* (red), HA-Ub-K6 (green), and DNA (blue). Arrows indicate the position of a bacterium in each channel. Images were collected at 100x magnification. Scale bars correspond to 10 μm.

C. Representative images of HeLa FcγRII cells infected with the indicated *L. pneumophila* strains at an MOI of 2 for 4 h. Fixed cells were stained for *L. pneumophila* (red), VCP (green), and DNA (blue). Arrows indicate the position of a bacterium in each channel. Images were collected at 100x magnification. Scale bars correspond to 10 μm.